Journal of The Electrochemical Society, **153** (4) A781-A786 (2006)
0013-4651/2006/153(4)/A781/6/$20.00 © The Electrochemical Society

Structural Characterization of the Surface-Modified $Li_xNi_{0.9}Co_{0.1}O_2$ Cathode Materials by MPO_4 Coating (M = Al, Ce, SrH, and Fe) for Li-Ion Cells

Hyunjung Lee,[a] Yoojung Kim,[a] Young-Sik Hong,[b] Yoojin Kim,[a,c] Min Gyu Kim,[c] Nam-Soo Shin,[c] and Jaephil Cho[a,*,z]

[a]*Department of Applied Chemistry, Kumoh National Institute of Technology, Gumi, Korea*
[b]*Department of Science Education, Seoul National University of Education, Seoul, Korea*
[c]*Beamline Research Division, Pohang Accelerator Laboratory, Pohang University of Science and Technology, Pohang, Korea*

Structural characterization of surface-modified $Li_xNi_{0.9}Co_{0.1}O_2$ cathodes ($x = 0.3$ and 0.15) using an MPO_4 coating (M = Al, Ce, SrH, and Fe) were investigated for their potential applications to Li-ion cells. MPO_4 nanoparticles that were precipitated from metal nitrate and $(NH_4)_2HPO_4$ in water at pH = 10 were coated on the cathodes via mixing and heat treatment at 700°C. The $CePO_4$ and $SrHPO_4$-coated $Li_{0.3}Ni_{0.9}Co_{0.1}O_2$ cathodes heat treated at 300°C were mainly made up of the rock-salt phase ($Fm3m$), while $AlPO_4$ and $FePO_4$-coated cathodes showed disordered $[Li_{1-x}(Ni,Co)_x]_{3b}[(Ni,Co)_y]_{3a}O_2$-type hexagonal structure ($R\bar{3}m$) with a cation mixing. However, when the x value decreased from 0.3 to 0.15, bare and coated cathodes which had a spinel ($Fd3m$) or hexagonal structure ($R\bar{3}m$) at $x = 0.3$ were transformed into a NiO-type rock-salt structure. $AlPO_4$-coated sample exhibited lowest degree of oxygen generation after 300°C annealing at $x = 0.15$, indicating the highest thermal stability among the bare and coated cathodes.
 [DOI: 10.1149/1.2172567]

Manuscript submitted August 25, 2005; revised manuscript received December 28, 2005.
Available electronically February 24, 2006.

There is substantial oxygen evolution $LiNiO_2$ above 200°C on account of its structural instability at the delithiated states,[1-6] and the amount of oxygen evolution was reported to relate to thermal stability; sometimes it triggers a thermal runaway.[1-9] In order to solve this problem, Ni cations were substituted with Co, Mn, Ti, Mg, Al, and Co, and the highest discharge capacity was observed at 4.3 V, but the thermal instability problem still remained.[10-14] Recently, there have been some studies aimed at determining if an $AlPO_4$ or SiO_x coating on the cathodes can control the rate of oxygen evolution from the cathode. Cho et al. reported that an $AlPO_4$ coating on $Li_xNi_{0.8}Co_{0.1}Mn_{0.1}O_2$ drastically decreased the rate of oxygen evolution at 4.5 V during the course of nail penetration, and the amount of oxygen was decreased by as much as 1/6 as a result of the coating.[15] However, the $AlPO_4$ coating layer appeared to disappear, which was in contrast to that observed with $LiCoO_2$, and a solid solution phase was instead formed from a reaction between the coating and bulk material. Similarly, Omanda et al. reported that SiO_x coating decreased the rate of oxygen evolution in the $LiNi_{0.8}Co_{0.2}O_2$ by 50%.[16]

However, only one study reported how the enhanced thermal stability of the coated cathodes was related to the structural changes at ambient temperatures. The bare and $AlPO_4$-coated Li_xCoO_2 materials showed a phase transition toward Co_3O_4 spinel when the x value decreased from 0.4 to 0.24, and the rate formation of the Co_3O_4 fraction of the $AlPO_4$-coated cathode was larger than that of the bare sample.[17]

Similar approaches to the above in delithiated Ni-based cathodes beyond 200°C have been reported. Lee et al. reported that layered $Li_{1-x}NiO_2$ decomposed to a spinel phase (cubic, $Fd3m$) at 220°C and was converted to a NiO-type rock-salt phase ($Fm3m$) at higher temperatures.[18] They also suggested that the thermal stability of the cathode could be achieved by stabilizing the spinel structure, which in turn blocked the phase transition to a rock-salt phase.[19] Hence, they believed that $Li_{0.5}Ni_{0.85}Co_{0.15}O_2$ was thermally stable due to the formation of a spinel phase at 300°C. However, more lithium deintercalation from this composition led to an increase in the proportion of the rock-salt phase. Therefore, $Li_{0.2}NiO_2$ was transformed into a rock-salt phase at 300°C. Guilmard et al. reported that $Li_{0.3}Ni_{1.02}O_2$ decomposed to a disordered spinel phase above 200°C and was converted to a disordered hexagonal structure ($R\bar{3}m$) with cation-mixing at 300°C.[20] Above 300°C, the rock-salt phase was reported to be dominant.

In this paper, we report the structural changes of the bare and surface-modified $Li_xNi_{0.9}Co_{0.1}O_2$ cathodes by using MPO_4 (M = Al, Ce, Fe, and SrH) at $x = 0.3$ and 0.15. Because the oxygen evolution from the cathode gets to start on the particle surface, surface modification is expected to affect structure stability depending on a coating material.

Experimental

The $Ni_{0.9}Co_{0.1}(OH)_2$ starting powders consisting of spherical particles (~13 μm in average diameter) were prepared by coprecipitation from a solution containing stoichiometric amounts of nickel/cobalt nitrates through the addition of NaOH and NH_4OH solutions in specially designed reactors at 50°C. The pH was maintained at 11.5 by controlling the NaOH concentration. $LiNi_{0.9}Co_{0.1}O_2$ was prepared by mixing stoichiometric amounts of 1.03:1 in $LiOH{\cdot}H_2O$ and $Ni_{0.9}Co_{0.1}(OH)_2$, followed by heat treatment at 700°C for 12 h in a stream of dried air. An excess of Li = 1.03 was used to compensate for the loss of Li during firing, and inductively coupled plasma-atomic emission spectroscopy (ICP-AES) analysis showed the Li stoichiometry after annealing to be $x = 1.01$. In order to coat the MPO_4 particles on the $LiNi_{0.8}Co_{0.1}Mn_{0.1}O_2$ cathodes, 3 g of $M(NO_3)_3{\cdot}9H_2O$ (M = Al, Fe, Sr, and Ce) and 1 g of $(NH_4)_2HPO_4$ were slowly dissolved in 20 g of water until a white MPO_4 nanoparticle suspension was observed (chemical formula of the precipitated nanoparticles was MPO_4 but the formula of the nanoparticles containing Sr was $SrHPO_4$). The pH of the solution was adjusted to 10. $LiNi_{0.9}Co_{0.1}O_2$ (50 g), ~13 μm in size were added to the coating solution and mixed thoroughly for 5 min. The slurry was then dried in an oven at 120°C for 6 h, and heat treated in a furnace at 700°C for 5 h.

The cathodes for the battery test cells were made from the active material (~25 mg), super-P carbon black (MMM, Belgium), and a polyvinylidene fluoride (PVdF) binder (Kureha Company, Japan) at a weight ratio of 94:3:3. A cathode slurry was prepared by thoroughly mixing an *N*-methyl-2-pyrrolidinone (NMP) solution with

* Electrochemical Society Active Member.
z E-mail: jpcho@kumoh.ac.kr

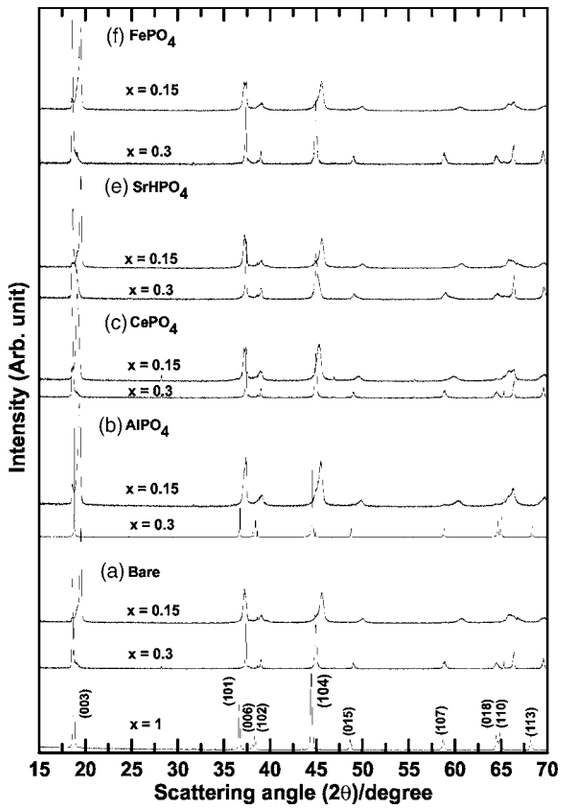

Figure 1. XRD patterns of the bare and MPO_4-coated $Li_xNi_{0.9}Co_{0.1}O_2$ cathodes (M = Al, Fe, Fe, SrH, and Ce), where $x = 0.3$ and 0.15.

PVdF, carbon black, and the powdery cathode-active material. The electrodes were prepared by coating the cathode slurry onto an Al foil, followed by drying at 130°C for 20 min. Coin-type battery-test cells (size 2016) containing a cathode, a Li metal anode, and a microporous polyethylene separator were prepared in a helium-filled glove box. The electrolyte used was 1 M $LiPF_6$ with ethylene carbonate/diethylene carbonate/ethyl-methyl carbonate (EC/DEC/EMC) (30:30:40 vol %) (Cheil Industries, Korea). After adding the electrolyte, the test cells were aged at room temperature for 24 h before beginning the electrochemical tests. The cells were initially charged to either 4.35 or 4.6 V, at a current of 10 mA/g, and were maintained at these voltages for 2 h by applying a constant voltage. The charged coin cells were transferred to an argon-filled glove box, and the cathode electrodes detached from the coin cells were scratched in order to collect the soaked cathode composite containing the electrolyte. The scratched electrodes were transferred into Al sample pans for sealing. The sealed sample pan was then heated to 300°C at a rate of 5°C/min, which was maintained at this temperature for 1 h, followed by slow cooling to room temperature.

Powder X-ray diffraction measurements were carried out using an M18XHF-SRA diffractometer (MAC Science Co.) with a Cu-target tube used for X-ray diffraction (XRD) measurement with a graphite monochromator. The X-ray photoelectron spectra were recorded with a Physical Electronics Quantum 2000 ESCA spectrometer with a Mg Kα anode (1253.6 eV) as the X-ray source operated at 24.1 W in a vacuum of $<10^{-8}$ Torr. The binding energy was corrected to the C 1s peak at 284.5 eV.

Results and Discussion

Figure 1 shows the XRD patterns of the bare and coated $Li_xNi_{0.9}Co_{0.1}O_2$ cathodes at $x = 1$, 0.3, and 0.15. XRD patterns of the coated samples before charging were identical to that of the bare sample. The profiles are all similar except for the peak positions, indicating that the hexagonal unit of $Li_xNi_{0.9}Co_{0.1O}O_2$ was maintained. Li et al. reported that the phase transition can be easily identified by the (003) peak, which changed from 18.6 to 19.6° when the *H*2 phase transformed to the *H*3 phase.[8] No other phases from the coating materials were detected. Table I shows the result of Rietveld analysis. The table shows that the Ni composition in the 3*b* lithium sites was <2%, indicating negligible cation mixing in the 3*a* and 3*b* sites even after coating. The well-splitting (018) and (110) peaks of the as-prepared samples indicate that there is little Ni cation migration to the lithium sites, which agrees with the Rietveld results. As generally observed for the bare and coated $Li_xNi_{0.9}Co_{0.1}O_2$ cathodes, there was a displacement to a higher diffraction angle and a large broadening of the diffraction lines when the *x* value decreased. For $x = 0.15$, completely different phenomena are observed, and the well-separated (018) and (110) peaks observed at $x = 0.3$ are merged into a single peak regardless of coating. This is due to a collapse of the interlayer distance. In addition, peaks broadening at $x = 0.15$ are associated with stacking faults in the cathode materials. In Ni-based

Table I. Rietveld analysis of the bare and MPO_4-coated $LiNi_{0.9}Co_{0.1}O_2$ cathodes (M = Al, Fe, SrH, and Ce). A formula of $[Li_{1-z}(Ni,Co)_z]_{3b}[(Ni,Co)_y]_{3a}O_2$ was assumed.

Sample	*a* (Å)	*c* (Å)	*z*	R_p	R_{wp}	R_B	R_e
Bare	2.873(3)	14.184(5)	0.0176	14.0	10.9	2.56	7.3
$AlPO_4$	2.872(6)	14.184(3)	0.0198	15.8	11.9	3.50	8.5
$CePO_4$	2.872(7)	14.182(4)	0.0290	17.1	13.4	4.24	8.6
$FePO_4$	2.872(5)	14.183(6)	0.0220	15.2	11.7	3.92	7.8
$SrHPO_4$	2.872(5)	14.185(3)	0.0240	16.3	12.7	4.12	8.6

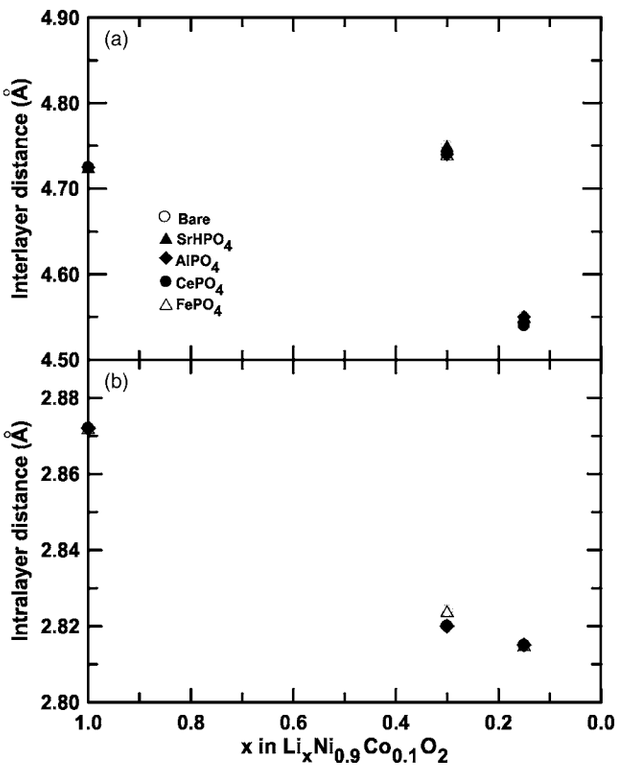

Figure 2. Distances (a) between the interlayers (one third of *c*-axis in the hexagonal unit cell) and (b) between intralayer neighbors (metal-metal distance) (*a*-axis in hexagonal cell).

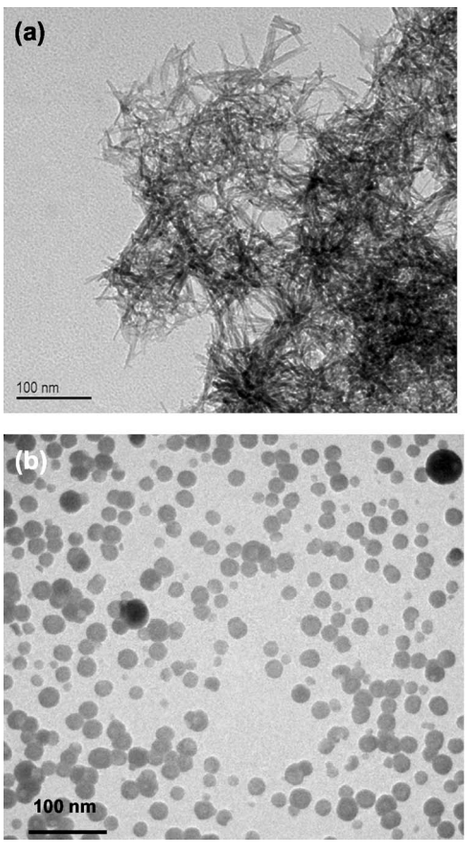

Figure 3. TEM images of (a) $CePO_4$ nanoparticles prepared at pH 3 and (b) $CePO_4$ nanoparticles prepared at pH 10.

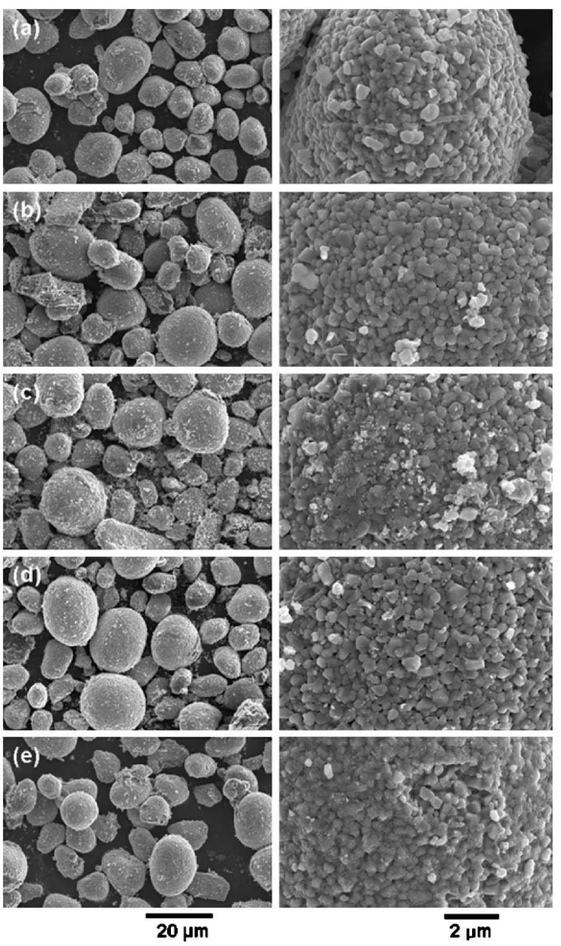

Figure 4. SEM images of the bare and MPO_4-coated cathodes: (a) bare; (b) $AlPO_4$; (c) $SrHPO_4$; (d) $FePO_4$; and (e) $CePO_4$.

cathode materials, O1-type stacking fault appeared at $x = 0$ in the O3-type ($R\bar{3}m$) oxygen packing, reported to induce such peak broadening.[21,22]

Figure 2 compares the lattice constants of the MPO_4-coated cathodes ($x = 0.3$ and 0.15), which are described as the distance between the interlayers (one third of *c*-axis in hexagonal unit cell) and the interlayer neighbors (metal-metal distance) (*a*-axis in hexagonal cell). The overall trend of the interlayer distance in both the bare and coated samples was similar to results reported by Arai et al.[23] The interlayer distance of the $Li_xNi_{0.9}Co_{0.1}O_2$ increased until $x = 0.3$ and then decreased considerably at $x = 0.15$. This was attributed to Ni^{3+} and Co^{3+} being in the low-spin states of $(t_{eg})^6(e_g)^1$ and $(t_{2g})^6(e_g)^0$, respectively.[24,25] When Ni^{3+} is oxidized to Ni^{4+}, the state becomes $(t_{eg})^6(e_g)^0$, which is the same as Co^{3+} (not oxidized) with no electron in the antibonding orbital. The distance between the transition metal and the oxygen (interlayer) bond would then shrink considerably.

Figure 3 shows the $CePO_4$ nanoparticles prepared at pH 3 (top) and pH 10 (bottom). In the case of $LiCoO_2$, MPO_4 nanoparticles were precipitated at pH~3,[26] but the pH was adjusted to 10 for $LiNi_{0.9}Co_{0.1}O_2$ due to Ni and Li dissolution under acidic conditions. The morphology of the MPO_4 nanoparticles at pH 10 was identical to those prepared at pH 3, and particle morphology was spherical with a size distribution between ~3 and 100 nm,[26] except for $CePO_4$, which shows a change in morphology from whiskers to spherical particles with a particle size of ~25 nm. Spherical shape of the coating materials is expected to lead to uniform coating layers.

Figure 4 shows scanning electron microscopy (SEM) images of the bare and coated cathodes after heat treatment at 700°C. The figure shows that surface morphology of the coated samples is similar to the bare sample, maintaining rock-shaped particles even after coating. Previous studies on the $AlPO_4$-coated $LiNi_{0.8}Co_{0.1}Mn_{0.1}O_2$ cathodes also showed a similar surface morphology after coating.[27] The surface morphology after coating should be different from that of the bare sample, but the surface morphologies of the MPO_4-coated $LiNi_{0.8}Co_{0.1}Mn_{0.1}O_2$ samples were similar to that of the bare sample, suggesting the coating layers had disappeared as a result of the formation of a solid solution from the reaction between MPO_4 and the surface of the bulk $LiNi_{0.8}Co_{0.1}Mn_{0.1}O_2$. This is further supported by TEM analysis of the bare and cross-sectioned $FePO_4$ and $CePO_4$-coated samples, as shown in Fig. 5, and expanded images in Fig. 5d and e correspond to 5b and c, respectively. Both transmission electron microscopy (TEM) images showed no presence of the coating layer in contrast to $LiCoO_2$, which exhibited clearly distinguishable coating layers.[26] The amorphous-like coating layers on the coated samples was epoxy-type glues.

X-ray photoemission spectroscopy (XPS) analysis of the Ni and Co elements in the bare and $CePO_4$-coated samples was carried out ln order to examine the possibility of a solid solution formation, as shown in Fig. 6. When the coating layer consists of $CePO_4$ only, Ni and Co should not be detected or drastic decrease of peak intensity is expected because of the coating layer. For instance, SiO_x coating layer on the $LiNi_{0.8}Co_{0.2}O_2$ cathode led to significant decrease in intensities of the Co $2P_{2/3}$ and Ni $2P_{3/2}$ peaks, compared with an uncoated sample.[16] However, $CePO_4$-coated sample shows no apparent intensity decreases of the Co $2P_{2/3}$ and Ni $2P_{3/2}$ peaks after

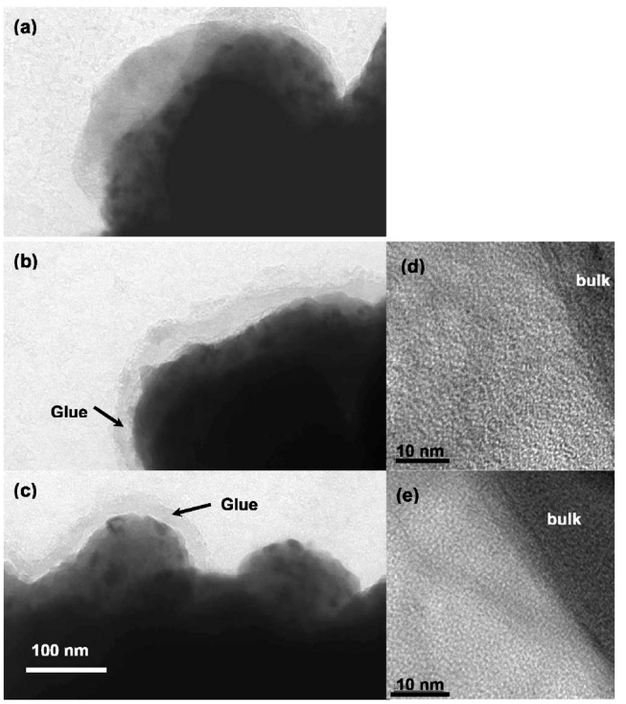

Figure 5. TEM images of the (a) bare; (b) cross-sectioned $FePO_4$; and (c) $CePO_4$-coated $LiNi_{0.9}Co_{0.1}O_2$ cathodes. (d) and (e) are expanded TEM images of (b) and (c), respectively. The outmost surface layer covered on the coated material is glue (indicated by arrows). Scale bar in (c) is also applied to (a) and (b).

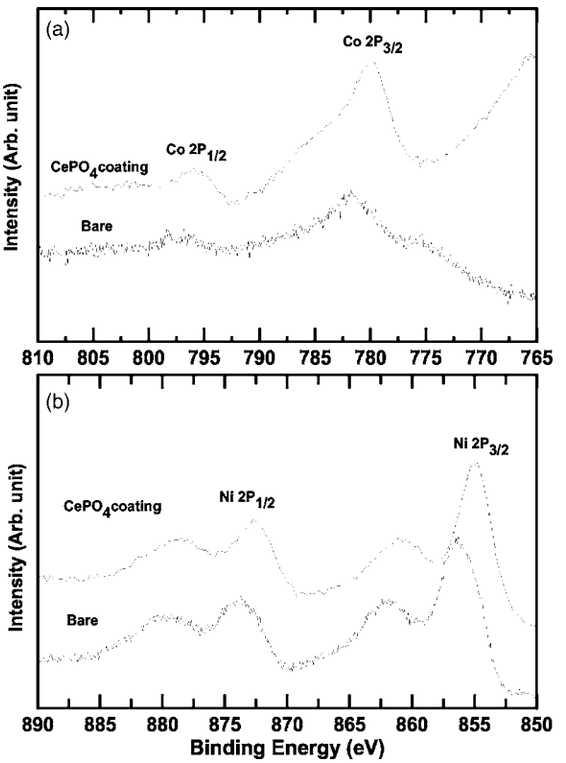

Figure 6. XPS of the (a) Co $2P_{1/2}$ and Co $2P_{3/2}$ of the bare and $CePO_4$-coated $LiNi_{0.9}Co_{0.1}O_2$ and (b) Ni2$P_{1/2}$ and Ni2$P_{3/2}$ of the bare and $CePO_4$-coated $LiNi_{0.9}Co_{0.1}O_2$.

coating, indicating the disappearance of the coating layer. Moreover, the figure shows that, after the $CePO_4$ coating, Co $2P_{1/2}$ and Ni $2P_{1/2}$ and Co $2P_{2/3}$ and Ni $2P_{3/2}$ shifted to a lower binding energy from the 782 and 856 eV to 780 and 855 eV, respectively, indicating that the bonding environment around the Co and Ni ions after coating was different from that before coating. The binding energies of the major Co $2P_{2/3}$ and Ni $2P_{3/2}$ peaks from typical of the energies are expected for Co^{3+} and Ni^{3+}, respectively. Shift of the peaks to lower binding energies is because Co and Ni atoms are bound to less electronegative element, such as Ce. Figure 7 showed XPS of P 2p and O 1s in the $CePO_4$ nanoparticle and bare, $CePO_4$-coated sample after annealing. After $CePO_4$ coating, P 2p peak shifted downward to 133.5 eV from 136 eV. Similarly, O 1s peak downshifted to 532 eV from 533 eV after coating. This reveals that P ion environment in the structure, opposite that in oxygen ions, is significantly changed. One possibility is substitution of P ions into the metal sites, not oxygen sites as a result of the solid solution formation.

Next, we investigate whether such MPO_4 coatings can influence the structural changes in the bare cathodes annealed at 300°C. Figure 8 shows the ex situ XRD patterns of the $x = 0.3$ in the bare and coated $Li_xNi_{0.9}Co_{0.1}O_2$ cathodes. Bare and $CePO_4$ and $SrHPO_4$-coated cathodes mainly consisted of the spinel ($Fd3m$) and NiO-type rock-salt phases ($Fm3m$). A similar phase transition was observed in the $Li_{0.3}Ni_{0.89}Al_{0.06}O_2$ and $Li_{1-x}Ni_{1+x}O_2$ annealed at 300°C.[20,28-33] The $R\bar{3}m$ hexagonal phase to the spinel phase occurs via the overall migration of 25% of the Ni^{4+} cations from the slab to the interlayer space, as well as through the displacement of the lithium ions from the octahedral to tetrahedral sites in the interlayer space.[32] This type of phase transition evolves an oxygen loss. The $AlPO_4$ and $FePO_4$-coated cathodes maintained the original hexagonal phase but showed a larger intensity of the (104) peak than the (003) peak, which is indicative of the formation of a $[Li_{1-x}(Ni,Co)_x]_{3b}[(Ni,Co)_{1-y}Li_y]_{3a}O_2$-type hexagonal structure

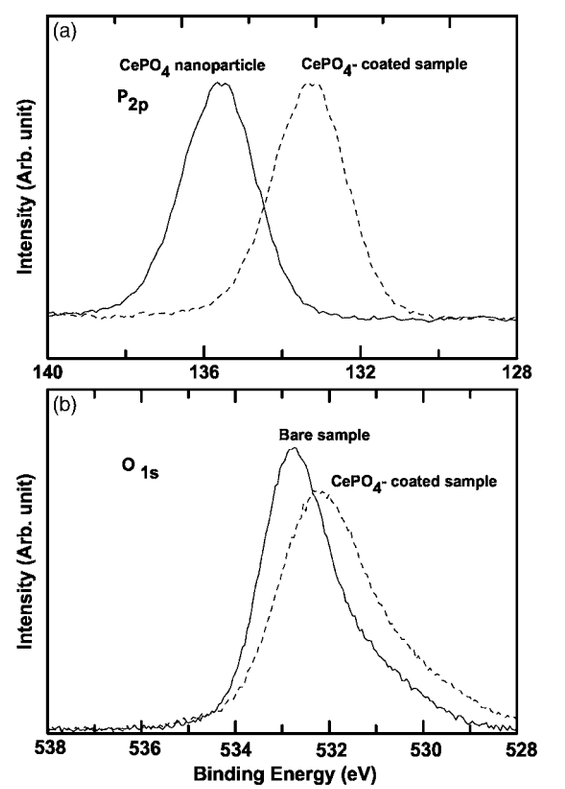

Figure 7. XPS showing (a) the P 2p of the $CePO_4$ nanoparticle and $CePO_4$-coated $LiNi_{0.9}Co_{0.1}O_2$ and (b) the O 1s of the bare and $CePO_4$-coated $LiNi_{0.9}Co_{0.1}O_2$.

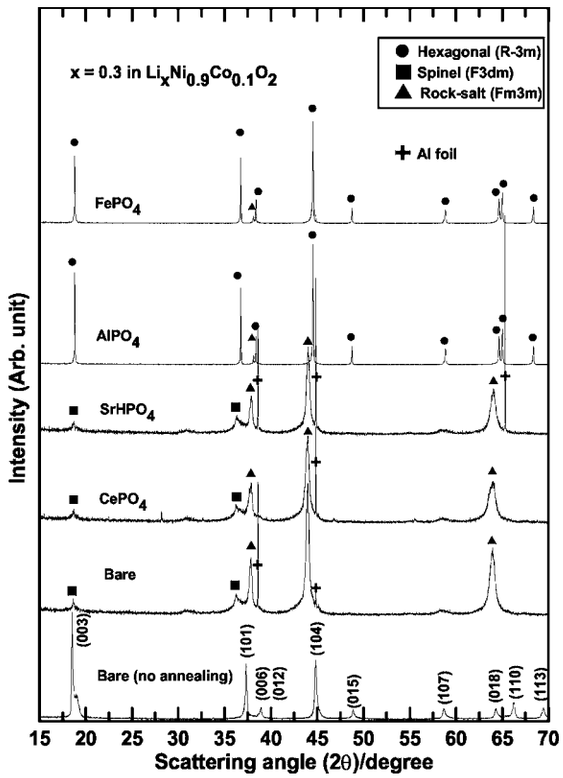

Figure 8. Ex situ XRD patterns of the bare and MPO_4-coated $Li_xNi_{0.9}Co_{0.1}O_2$, in which $x = 0.3$ after annealing at 300°C for 1 h.

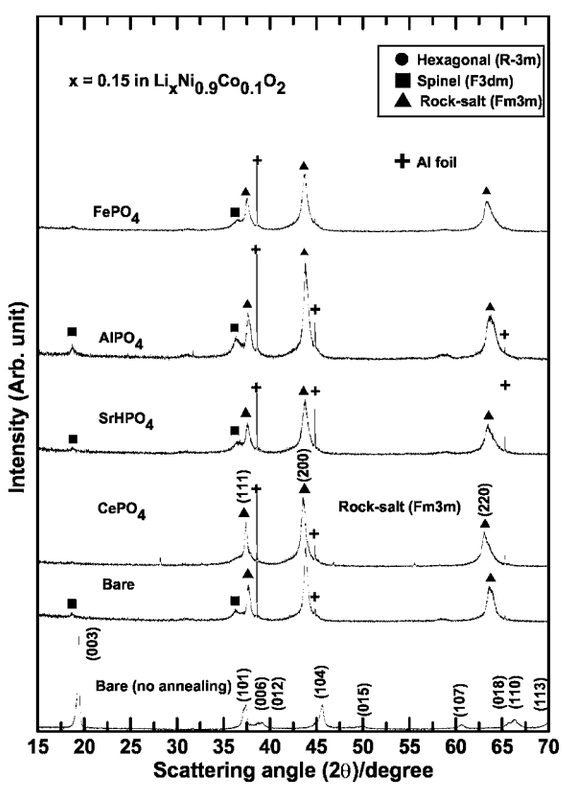

Figure 9. Ex situ XRD patterns of the bare and MPO_4-coated $Li_xNi_{0.9}Co_{0.1}O_2$, in which $x = 0.15$ after annealing at 300°C for 1 h.

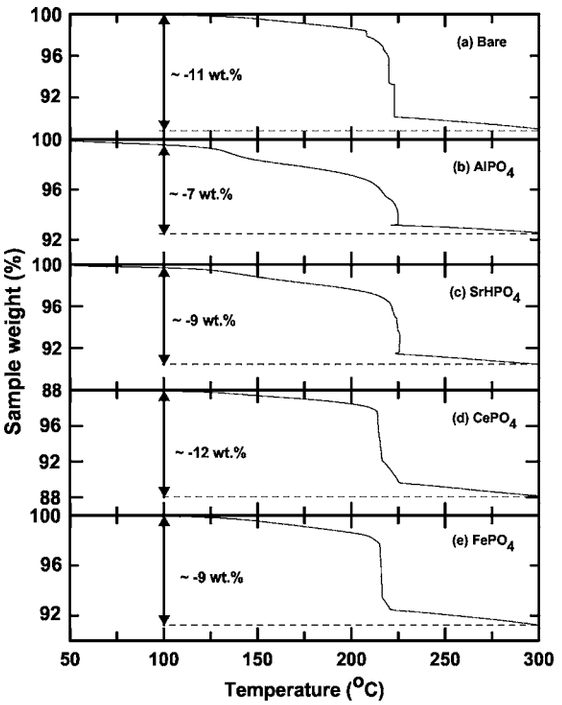

Figure 10. TGA of the bare and MPO_4-coated $Li_xNi_{0.9}Co_{0.1}O_2$ cathodes between 100 and 300°C, where $x = 0.15$.

($R\bar{3}m$) with a significant cation mixing. This behavior indicates $AlPO_4$ and $FePO_4$ coating is very effective in retarding the oxygen loss. However, more lithium removal from $Li_{0.3}Ni_{0.9}Co_{0.1}O_2$ may lead to much oxygen loss from the phase irrespective of coating because the phase mostly contained the nickel 4+ ions, which are very unstable. Accordingly, these Ni ions are apt to reduce to the divalent state, with the loss of oxygen. Figure 9 shows the ex situ XRD patterns of $x = 0.15$ in the bare and coated $Li_xNi_{0.9}Co_{0.1}O_2$ annealed at 300°C. It is clear that $CePO_4$-coated sample was completely transformed into the rock-salt phase. The others still showed mixed phases of the rock-salt phase and the spinel phase. Because the phase transition to a rock-salt phase releases the largest amounts of oxygen,[18,19] $CePO_4$-coated sample that have only a rock-salt phase should show the highest amount of oxygen generation. Further, more oxygen generation is indicative of the more thermal instability of the cathode. Figure 10 exhibits the amount of oxygen loss from the bare and coated $Li_{0.15}Ni_{0.9}Co_{0.1}O_2$ cathodes between 100 and 300°C. Its loss depends on the coating material and increases in the order of $AlPO_4 < FePO_4 \approx SrHPO_4 <$ bare $\approx CePO_4$, indicating that $AlPO_4$-coated sample is the most thermally stable one. The fact that amount of oxygen loss from the $CePO_4$-coated cathode is similar to the bare one indicates that the $CePO_4$ coating has no effect on improving thermal stability of the cathode.

Conclusion

Structural changes of the coated cathodes at 300°C were influenced by the coating materials, depending on x value in $Li_xNi_{0.9}Co_{0.1}O_2$. Moderate lithium removal ($x = 0.3$) resulted in structural stability for $AlPO_4$ and $FePO_4$-coated cathodes that maintained an original layered structure in opposite to bare, and $CePO_4$-, $SrHPO_4$-coated cathodes. However, more lithium removal from $x = 0.3$ led to formation of the rock-salt structure, irrespective of coating. Among the bare and coated samples, $AlPO_4$-coated sample showed the smallest amount of oxygen evolution from the cathode, indicating the most thermally stable coating material.

Acknowledgments

The authors are grateful to authorities at the Pohang Light Source (PLS) for the XRD measurements. The experiments at the PLS were supported in part by Korea MOST and POSTECH. This study was supported by University IT Research Project.

Kumoh National Institute of Technology assisted in meeting the publication costs of this article.

References

1. S. H. Park, K. S. Park, Y. K. Sun, K. S. Nahm, Y. S. Lee, and M. Yoshio, *Electrochim. Acta*, **46**, 1215 (2001).
2. M. Yoshio, H. Noguchi, J.-I. Itoh, M. Okada, and T. Mouri, *J. Power Sources*, **90**, 176 (2000).
3. C. Nayoze, F. Ansart, C. Laberty, J. Sarrias, and A. Rousset, *J. Power Sources*, **99**, 54 (2001).
4. J. Cho, H. Jung, Y. Park, G. Kim, and H. S. Lim, *J. Electrochem. Soc.*, **147**, 15 (2000).
5. J. Cho, G. Kim, and H. S. Lim, *J. Electrochem. Soc.*, **146**, 3571 (1999).
6. Z. Zhang, D. Fouchard, and J. R. Rea, *J. Power Sources*, **70**, 16 (1998).
7. A. Ueda and T. Ohzuku, *J. Electrochem. Soc.*, **141**, 2010 (1994).
8. W. Li, J. N. Reimers, and J. R. Dahn, *Solid State Ionics*, **67**, 123 (1993).
9. J. Cho, T. J. Kim, Y. Kim, and B. Park, *Electrochem. Solid-State Lett.*, **4**, A159 (2001).
10. W. Li and J. C. Currie, *J. Electrochem. Soc.*, **144**, 2773 (1997).
11. C. Delmas, I. Saadoune, and A. Rougier, *J. Power Sources*, **44**, 595 (1993).
12. Y. Gao, M. V. Yakovleva, and W. B. Ebner, *Electrochem. Solid-State Lett.*, **1**, 117 (1998).
13. Y. Nishida, K. Nakane, and T. Satoh, *J. Power Sources*, **68**, 561 (1997).
14. J. Cho, *Chem. Mater.*, **13**, 4537 (2001).
15. J. Cho, T.-J. Kim, J. Kim, M. Noh, and B. Park, *J. Electrochem. Soc.*, **151**, A1899 (2004).
16. H. Omanda, T. Brousse, C. Marhic, and D. M. Schleich, *J. Electrochem. Soc.*, **151**, A922 (2004).
17. Y. Lee, M. G. Kim, J. Kim, Y. Kim, and J. Cho, *J. Electrochem. Soc.*, **152**, A1824 (2005).
18. K. K. Lee, W. S. Yoon, K.-B. Kim, K. Y. Lee, and S.-T. Hong, *J. Power Sources*, **97–98**, 321 (2001).
19. K. K. Lee, W. S. Yoon, and K. B. Kim, *J. Electrochem. Soc.*, **148**, A1164 (2001).
20. M. Guilmard, L. Croguennec, D. Denux, and C. Delmas, *Chem. Mater.*, **15**, 4476 (2003).
21. H. Arai, M. Tsuda, K. Saito, M. Hayashi, and Y. Sakurai, *Solid State Ionics*, **109**, 295 (1998).
22. L. Croguennec, C. Pouillerie, A. N. Mansour, and C. Delmas, *J. Mater. Chem.*, **11**, 131 (2001).
23. H. Arai, S. Okada, Y. Sakurai, and J. Yamaki, *J. Electrochem. Soc.*, **144**, 3117 (1997).
24. W. Ebner, D. Fouchard, and L. Xie, *Solid State Ionics*, **69**, 238 (1994).
25. T. Ohzuku, A. Ueda, M. Nagayama, Y. Iwakoshi, and H. Komori, *Electrochim. Acta*, **38**, 1159 (1993).
26. J. Kim, M. Noh, J. Cho, H. Kim, and K. Kim, *J. Electrochem. Soc.*, **152**, A1142 (2005).
27. J. Cho, H. Kim, and B. Park, *J. Electrochem. Soc.*, **151**, A1707 (2004).
28. Y.-I. Jang, N. J. Dudney, D. A. Blom, and L. F. Allard, *J. Electrochem. Soc.*, **149**, A1442 (2002).
29. G. G. Amatucci, J.-M. Tarascon, and L. C. Klein, *Solid State Ionics*, **83**, 167 (1996).
30. Y. J. Kim, J. Cho, T.-J. Kim, and B. Park, *J. Electrochem. Soc.*, **150**, A1723 (2003).
31. A. M. Andersson, D. P. Abraham, R. Haasch, S. MacLaron, J. Liu, and K. Amine, *J. Electrochem. Soc.*, **149**, A1358 (2002).
32. M. G. S. R. Thomas, W. I. F. David, and J. B. Goodenough, *Mater. Res. Bull.*, **20**, 1137 (1985).
33. J. Morales, C. Perez-Vicente, and J. L. Tirado, *Mater. Res. Bull.*, **25**, 623 (1990).